


Arabidopsis mRNA export factor MOS11: molecular interactions and role in abiotic stress responses

Amelie Rödel¹, Ina Weig¹, Sophie Tiedemann¹, Uwe Schwartz², Gernot Längst³, Christoph Moehle⁴, Marion Grasser¹ and Klaus D. Grasser¹ 

¹Cell Biology & Plant Biochemistry, Biochemistry Center, University of Regensburg, Universitätsstr. 31, D-93053, Regensburg, Germany; ²NGS Analysis Center, Biology and Pre-Clinical Medicine, University of Regensburg, Universitätsstr. 31, D-93053, Regensburg, Germany; ³Institute for Biochemistry III, Biochemistry Center, University of Regensburg, Universitätsstr. 31, D-93053, Regensburg, Germany; ⁴Center of Excellence for Fluorescent Bioanalytics (KFB), University of Regensburg, Am Biopark 9, D-93053, Regensburg, Germany

Summary

Author for correspondence:
Klaus D. Grasser
Email: klaus.grasser@ur.de

Received: 20 November 2023
Accepted: 1 April 2024

New Phytologist (2024)
doi: 10.1111/nph.19773

Key words: *Arabidopsis thaliana*, MOS11, mRNA export, nucleocytoplasmic transport, protein interactions, RNA-binding protein, TREX.

- Transcription and export (TREX) is a multi-subunit complex that links synthesis, processing and export of mRNAs. It interacts with the RNA helicase UAP56 and export factors such as MOS11 and ALYs to facilitate nucleocytoplasmic transport of mRNAs. Plant MOS11 is a conserved, but sparsely researched RNA-binding export factor, related to yeast Tho1 and mammalian CIP29/SARNP.
- Using biochemical approaches, the domains of *Arabidopsis thaliana* MOS11 required for interaction with UAP56 and RNA-binding were identified. Further analyses revealed marked genetic interactions between *MOS11* and *ALY* genes. Cell fractionation in combination with transcript profiling demonstrated that MOS11 is required for export of a subset of mRNAs that are shorter and more GC-rich than MOS11-independent transcripts.
- The central α -helical domain of MOS11 proved essential for physical interaction with UAP56 and for RNA-binding. MOS11 is involved in the nucleocytoplasmic transport of mRNAs that are upregulated under stress conditions and accordingly *mos11* mutant plants turned out to be sensitive to elevated NaCl concentrations and heat stress.
- Collectively, our analyses identify functional interaction domains of MOS11. In addition, the results establish that mRNA export is critically involved in the plant response to stress conditions and that MOS11 plays a prominent role at this.

Introduction

In eukaryotic cells, pre-mRNAs are synthesised by RNA polymerase II within the cell nucleus. The pre-mRNAs undergo a series of processing/maturation steps that partially occur co-transcriptionally before transcript synthesis is completed. The major processing steps comprise m⁷G capping of the 5' end, intron removal by the spliceosome and 3' end endonucleolytic cleavage and addition of the poly(A) tail (Howe, 2002; Darnell, 2013). Before cytosolic ribosomes can translate the mRNAs into proteins, they must be exported from the nucleus. Nuclear export of mature mRNAs to the cytosol occurs through nuclear pore complexes and is mediated by a variety of proteins that have been recruited to the mRNAs (Köhler & Hurt, 2007; Wickramasinghe & Laskey, 2015).

A central function in linking RNA polymerase II transcription and pre-mRNA processing with mRNA export is executed by the transcription and export (TREX) complex. TREX consists of a hexameric core termed THO that associates with various combinations of additional proteins giving rise to alternative versions of TREX (Katahira, 2012; Heath *et al.*, 2016). An important interactor of THO is the DEAD-box RNA helicase UAP56 (Sub2 in

yeast), which has RNA-stimulated ATPase and RNA unwinding activity (Shen, 2009; Heath *et al.*, 2016). UAP56 is required for the contact with further export factors including ALY (Yra1 in yeast) and CIP29/SARNP (Tho1 in yeast) (Katahira, 2012; Heath *et al.*, 2016). Recently, the three-dimensional structure of various versions of yeast and mammalian TREX complexes has been uncovered, revealing that, for instance, a THO-UAP56 tetramer forms the core of human TREX (Pühringer *et al.*, 2020; Schuller *et al.*, 2020; Xie *et al.*, 2021; Pacheco-Fiallos *et al.*, 2023). Ultimately, TREX components recruit the mRNA export receptor that mediates interactions with nucleoporins of the nuclear pore complex, resulting in nucleocytoplasmic translocation of the mRNP (Heath *et al.*, 2016; Ashkenazy-Titelman *et al.*, 2020).

Compared with yeast and metazoa, little is known about the plant mRNA export pathway, including the fact that the export receptor(s) are unknown. They are conserved between yeast and mammals, but surprisingly, they are not encoded in plant genomes (Xu & Meier, 2008; Merkle, 2011; Gaouar & Germain, 2013; Ehrnsberger *et al.*, 2019a). As demonstrated by proteomics analysis, the THO core of *Arabidopsis* TREX resembles the composition of metazoan THO rather than that of the

yeast complex (Yelina *et al.*, 2010). Mediated by direct interactions with the RNA helicase UAP56, the export factors ALY1–4, UIEF1/2 and MOS11 (orthologue of yeast Tho1 and mammalian CIP29/SARNP) can be part of *Arabidopsis* TREX (Kammel *et al.*, 2013; Sørensen *et al.*, 2017; Pfaff *et al.*, 2018; Ehrnsberger *et al.*, 2019b). Based on *in situ* hybridisation analyses using oligo(dT) probes, some THO subunits were shown to be involved in mRNA export as in the respective mutant plants mRNAs accumulate within cell nuclei (Pan *et al.*, 2012; Xu *et al.*, 2015; Sørensen *et al.*, 2017). Similarly, the UAP56-associated factors MOS11, ALY1–4 and UIEF1/2 (Germain *et al.*, 2010; Pfaff *et al.*, 2018; Ehrnsberger *et al.*, 2019b) are required for efficient mRNA export. *MOS11* was originally identified in a genetic screen as suppressor of the *Arabidopsis* autoimmune mutant *snc1* (*modifier of snc1, 11*) and *MOS11* proved to be a nuclear protein with similarity to CIP29/SARNP (Germain *et al.*, 2010). Compared with wild-type (WT) plants, *mos11* mutants are phenotypically mildly affected, but they exhibit an mRNA export defect resulting in accumulation of mRNAs in nuclei (Germain *et al.*, 2010), that is increased in double-mutants deficient in *MOS11* and the THO subunit *TEX1* (Sørensen *et al.*, 2017). Recently, it was discovered that *MOS11* (and *ALYs*) are also involved in the nucleocytoplasmic transport of mRNAs of the pararetrovirus CaMV in *Arabidopsis* and that *mos11* (and *aly*) mutants are partially resistant to CaMV infection (Kubina *et al.*, 2021).

Since the RNA-binding properties of the *Arabidopsis* mRNA export factor *MOS11* and its molecular interactions with the RNA helicase UAP56 have not been studied in detail, we have investigated these aspects using full-length *MOS11* in comparison with various truncated proteins. To identify mRNAs, whose export is affected in *mos11* plants, we have profiled mRNAs isolated from nucleus vs cytosol of *mos11* and WT plants. In view of the moderate phenotypic impairment of *mos11* plants under normal growth conditions, we have exposed *mos11* plants to abiotic stress, demonstrating that *MOS11* and mRNA export are critical for proper stress response.

Materials and Methods

Plant material

Seeds of *Arabidopsis thaliana* (L.) Heynh. (ecotype Col-0) were stratified in darkness for 48 h at 4°C, and plants were grown and propagated at 21°C on soil in a phytochamber or on Murashige and Skoog (MS, 1962) medium in plant incubators (PolyKlima) under long-day conditions (16 h : 8 h, 21°C : 18°C, light : dark) (Antosz *et al.*, 2020; Michl-Holzinger *et al.*, 2022). In some experiments, the 0.5× MS medium was supplemented with 100 mM NaCl (Obermeyer *et al.*, 2022). Heat stress (HS) experiments (37°C) were conducted 14 d after stratification for 48 h, and the recovery was documented 7 d after HS (Obermeyer *et al.*, 2023). The T-DNA insertion lines were obtained from the Nottingham Arabidopsis Stock Centre (<https://arabidopsis.info/>) and were previously reported *mos11-2* (Germain *et al.*, 2010), *aly1-1*, *aly2-1*, *aly3-1* and *aly4-1* (Pfaff

et al., 2018). Double and triple mutants were generated by genetic crossing as previously described (Lolas *et al.*, 2010; Markusch *et al.*, 2023). *Agrobacterium*-mediated plant transformation, selection of primary transformants, characterisation of transgenic lines and PCR-based genotyping of plants using primers specific for DNA insertions and target genes (Supporting Information Table S1) as well as propagation and examination for consistent phenotype were performed as previously described (Antosz *et al.*, 2020; Michl-Holzinger *et al.*, 2022). All phenotypic analyses were performed independently at least twice, and representative examples are shown that were documented as previously described (Lolas *et al.*, 2010; Michl-Holzinger *et al.*, 2022).

Plasmid constructions

The required gene or cDNA sequences were amplified by PCR with KAPA DNA polymerase (PeqLab) using *A. thaliana* genomic DNA or cDNA as template and the primers (providing also the required restriction enzyme cleavage sites) listed in Table S1. The PCR fragments were inserted into suitable plasmids using standard methods. All plasmid constructions were checked by DNA sequencing, and details of the plasmids generated in this work are summarised in Table S2.

Production of recombinant proteins

Full-length *MOS11* and truncated versions of the protein (Table S2) were expressed in *Escherichia coli* using plasmid pQE9 (Qiagen) driving the expression of the *MOS11* proteins fused to a 6xHis-tag. The proteins were isolated from *E. coli* lysates by metal-chelate affinity chromatography using Ni-NTA beads (Qiagen) as previously described (Kammel *et al.*, 2013). Eluted *MOS11* proteins were further purified by FPLC ion exchange chromatography using a Resource S column (GE Healthcare, Freiburg, Germany) equilibrated in buffer D (10 mM sodium phosphate, pH 9.0, 1 mM EDTA, 1 mM DTT, 0.5 mM PMSF). Proteins were eluted with a linear gradient of 0–1 M NaCl in buffer D and *MOS11* containing fractions were pooled and passed through PD-10 columns (GE Healthcare) changing to protein buffer D. Finally, proteins were characterised by SDS-PAGE in combination with Coomassie staining and by mass spectrometry.

Circular dichroism (CD)

Purified recombinant *MOS11* proteins (10 µM) were analysed using a Jasco J-815 CD spectropolarimeter in a wavelength range of 190–260 nm using a 0.02-cm cell as previously described (Michl-Holzinger *et al.*, 2022).

MicroScale Thermophoresis (MST) binding assay

MicroScale Thermophoresis (MST) binding experiments were carried out essentially as previously described (Pfaff *et al.*, 2018) with 100 nM 25-nt Cy3-labelled ssRNA oligonucleotides (Table S1). MST measurements were performed in protein

buffer D with a range of protein concentrations at 25°C on a Monolith NT.115 device (NanoTemper Technologies, München, Germany).

ATPase assay

ATPase activity was examined with an adjusted protocol for phosphate determination via malachite green adapted from (Lanzetta *et al.*, 1979). 0.25 µM of UAP56, 10 mM ATP and 2.5 nM 13-nt RNA were incubated in 25 µl of ATPase assay reaction buffer at 28°C for 30 min. Twenty microlitres of the reaction mix was added to 80 µl of ATPase colour reagent in a 96-microwell plate and incubated at RT for 2 min. Ten microlitres of 34% (w/v) citric acid was added, and the samples were incubated at RT for 10 min, before the absorption of the samples was measured at a wavelength of 620 nm. For each assay, the corresponding blank sample lacking ATP was prepared and the samples were measured in triplicates along with respective blanks.

Helicase assay

In vitro RNA unwinding assays with 13-nt dsRNA were performed as previously described (Kammel *et al.*, 2013). Reaction products were treated with proteinase K and analysed in 1 × TBE on 16% polyacrylamide gels. Boiling of the dsRNA served as a control for strand separation. Finally, the Cy3-labelled RNA was visualised using a ChemiDoc Imaging System (Bio-Rad).

GST pull-down assays

Protein interaction assays using bait proteins fused to glutathione S transferase (GST) with putatively interacting proteins were performed essentially as previously described (Michl-Holzinger *et al.*, 2022; Markusch *et al.*, 2023). Proteins were incubated for 30 min in reaction buffer (25 mM Hepes pH 7.5, 150 mM KCl, 5% glycerol, 0.05% NP-40, 8 mM MgCl₂, 1.25 mM ATP and 0.2 mM PMSF) in a total volume of 150 µl, before eluted proteins (along with input samples) were loaded onto glutathione sepharose beads. Proteins were analysed by SDS-PAGE and Coomassie staining, and by immunoblotting using an antibody specific for the 6×-His-tag detecting putative interaction partners.

Yeast two-hybrid assays

Yeast two-hybrid assays were performed according to the manufacturer (Takara, Saint-Germain-en-Laye, France) as previously described (Pfaff *et al.*, 2018; Ehrnsberger *et al.*, 2019b). Yeast cells of the strain AH109 were co-transformed with pGBKT7 and pGADT7 plasmids (Table S1) and grown at 30°C on SD/-Leu/-Trp, SD/-Leu/-Trp/-His and SD/-Ade/-Leu/-Trp/-His medium for 2 d.

Förster resonance energy transfer (FRET)

FRET acceptor photobleaching (FRET-APB) was performed in *Agrobacterium*-infiltrated *Nicotiana benthamiana* leaves as

previously described (Pfaff *et al.*, 2018; Ehrnsberger *et al.*, 2019b) using a LSM 980 Airyscan 2 microscope (Zeiss). eGFP was excited with an Argon laser at 488 nm, and mCherry was excited/bleached with an DPSS laser at 561 nm. For acceptor bleaching, a circular area of 9 µm was bleached at 100% laser power (561 nm) for 15 iterations. The bleaching intensity was set to 50%. Twenty-five cycles were performed. For each replicate, 8–12 nuclei were sampled. Protein interactions were quantified with their mean FRET efficiencies.

Confocal laser scanning microscopy (CLSM)

Expression and localisation of mCherry and eGFP fusion proteins in *Agrobacterium*-infiltrated *N. benthamiana* leaf cells was analysed using a LSM 980 Airyscan 2 instrument (Zeiss) equipped with a 10× NA 0.3, a 20× NA 0.3, a 40× oil 1.3 or 63× oil NA 1.3 objective, as previously described (Markusch *et al.*, 2023). eGFP was excited with an Argon laser at 488 nm, mCherry was excited using a DPSS laser at 561 nm. The emission of eGFP or mCherry was detected at 500–550 nm or 570–620 nm.

Whole mount *in situ* hybridisation

The relative distribution of bulk mRNA in nuclei and cytosol was analysed in roots of 6-d-old seedlings grown on solid MS medium as previously described (Pfaff *et al.*, 2018; Ehrnsberger *et al.*, 2019b). Hybridisation was performed with an Alexa Fluor 488-labelled 48-nt oligo(dT) probe and analysed using confocal laser scanning microscopy with a Leica SP8 microscope.

Isolation of RNA, cDNA synthesis and analysis by qPCR

Nuclear and cytoplasmic fractions were prepared from rosettes of 14-d plants adapting a previously described protocol based on differential centrifugation (Park *et al.*, 2005). RNA was isolated from nuclear and cytoplasmic fractions using the RNeasy Plant Mini Kit (Qiagen). After DNase treatment, reverse transcription was performed using 1.5 µg of RNA, random hexameric primers and 200 U Reverse Transcriptase (Thermo Fisher Scientific, München, Germany) as previously described (Pfaff *et al.*, 2018). Subsequent analysis by qPCR was performed as previously described (Obermeyer *et al.*, 2022, 2023).

RNA-seq and data analysis

RNA was isolated from the nuclear and cytoplasmic fractions as described above. Additionally, the ERCC RNA Spike-In Mix (VWR, Darmstadt, Germany) was added to the isolated RNAs to control for the technical performance of library preparation and subsequent sequencing (Jiang *et al.*, 2011). Library preparation and RNA-seq were performed at the Genomics Core Facility (University of Regensburg, www.kfb-regensburg.de), employing the following modules: NuGEN Universal Plus RNA-Seq with NuQuant User Guide v3 (Tecan Genomics, Crailsheim, Germany) in combination with Arabidopsis rRNA AnyDeplete

module, the Illumina NextSeq 2000 System (Illumina, San Diego, CA, USA) and the KAPA Library Quantification Kit-Illumina/ABI Prism (Roche Sequencing Solutions, Penzberg, Germany). To remove PCR duplicates from the analysis, unique molecular identifiers (UMIs) were attached to the sequencing barcodes (Smith *et al.*, 2017). Equimolar amounts of each library were sequenced on an Illumina NextSeq 2000 instrument controlled by the NEXTSEQ 2000 Control Software (NCS, v.1.4.0.39521), using two 50 cycles P3 Flow Cells with the dual index, paired-end run parameters. Image analysis and base calling were done by the REAL TIME ANALYSIS Software (RTA, v.3.9.2). The resulting ‘.cbl’ files were converted into ‘.fastq’ files with the BCL2FASTQ (v.2.20) software.

Quality control was performed using FASTQC (v.0.11.9) and MULTIQ (v.1.11) (Ewels *et al.*, 2016). After the initial quality assessment, the UMIs were extracted and added to the header for each read using umi_tools extract (v.1.1) (Smith *et al.*, 2017). The remaining reads were mapped to the TAIR10 genome (Lamesch *et al.*, 2012) and ERCC sequences using STAR (v.2.7.8a, ‘--outFilterType BySJout --outFilterMultimapNmax 20 --alignSJoverhangMin 8 --alignSJDBoverhangMin 1 --outFilterMismatchNmax 999 --alignIntronMin 10 --alignIntronMax 1000000 --outFilterMismatchNoverReadLmax 0.04 --outSAMmultNmax 1 --outMultimapperOrder Random’). After tagging duplicated sequences using PICARD MARKDUPLICATES (v.2.21.8) (<https://broadinstitute.github.io/picard/>), the UMIs were used to remove technical duplicates using umi_tools (v.1.1). For the differential gene expression analysis, the resulting reads from the pipeline outlined above were used to create a count table using the FEATURECOUNTS function of the rsubread package (v.1.6.3) (Liao *et al.*, 2019), which was then analysed using the R BIOCONDUCTOR package DESEQ2 (v.1.38.3) (Love *et al.*, 2014). Genes encoded on the mitochondrial or chloroplast DNA were removed before the analysis. To determine transcripts, whose export is affected in *mos11* mutants, a likelihood ratio test (LRT) was used. The full model $\sim \text{compartment} + \text{genotype} + \text{compartment:genotype}$ was compared with the reduced model $\sim \text{compartment} + \text{genotype}$. Differentially distributed genes were defined using an FDR of 5% and clustered after *z*-score normalisation using *k*-means.

Gene set over-representation analysis was carried out using the Metascape online tool (Zhou *et al.*, 2019). Selected over-represented terms from Metascape analysis were visualised using the Bioconductor package CLUSTERPROFILER (Wu *et al.*, 2021).

Results

The central helical domain of MOS11 is required for interaction with UAP56 and RNA, while N-/C-terminal regions enhance RNA-binding

Arabidopsis MOS11 shares amino acid sequence similarity with mammalian CIP29 (also known as SARNP) and yeast Tho1 (Germain *et al.*, 2010), but MOS11 lacks the N-terminal SAP domain (Aravind & Koonin, 2000) found in CIP29 and Tho1 (Jacobsen *et al.*, 2016). Aligning MOS11 with the amino acid sequences of

putative orthologues from mono- and dicot species revealed striking conservation of the central part of the proteins, whereas the N- and C-terminal regions are rather diverse (Fig. S1). In view of a high-resolution NMR structure of Tho1 (Jacobsen *et al.*, 2016), it became clear that the conserved central regions mostly correspond to the α -helices identified in the C-terminal region of Tho1 (Fig. S2a). While the domain in Tho1 consists of two antiparallel α -helices that are connected by a structured loop, and whose helices are packed against each other by hydrophobic faces, this domain is duplicated in MOS11 and its plant (and mammalian) orthologues (Jacobsen *et al.*, 2016). Thus, in the plant sequences, the first helix-turn-helix motif consists of helices $\alpha 1/\alpha 2$ and the second motif consists of helices $\alpha 3/\alpha 4$ (Figs S1, S2a). Strikingly, each α -helix ends with a glycine residue that is preceded by a phenylalanine (Fig. S1). Using helices $\alpha 1/\alpha 2$ and $\alpha 3/\alpha 4$ of MOS11 for structure homology-modelling revealed that the pairs of helices each exhibit an organisation of antiparallel α -helices, connected by a loop (Fig. S2b), thus resembling the corresponding structure of Tho1 (Jacobsen *et al.*, 2016). Additionally, the protein sequence alignment revealed a fifth conserved motif that appears to be specific for plant MOS11 orthologues and which according to structure predictions may represent another α -helix (Fig. S2). To study molecular interactions of MOS11, the full-length protein and truncated versions were analysed (Fig. S3a). The MOS11 proteins were expressed as 6xHis-tagged proteins in *E. coli* and purified (Fig. S3b). Analysis by circular dichroism (CD) spectroscopy of full-length MOS11 and of MOS11 Δ NC (lacking the N- and C-terminal regions) yielded spectra consistent with α -helical structure, while the spectrum of MOS11 Δ α (lacking the central α -helical region) mostly reflects random coil (Fig. S3c). Together, this indicates that the central part, which MOS11 has in common with yeast Tho1 and mammalian CIP29, indeed is α -helical.

MOS11 directly interacts with UAP56 *in vivo* and *in vitro* (Kammel *et al.*, 2013; Sørensen *et al.*, 2017). To identify the part of MOS11 that is required for the interaction with UAP56, the yeast two-hybrid assay was used. As expected, full-length MOS11 fused to the activation domain clearly interacted with UAP56 fused to the DNA-binding domain (Fig. 1a). Analysis of truncated proteins demonstrated that MOS11 Δ NC interacted with UAP56, whereas no interaction was observed with MOS11 Δ α . To assess the protein interaction *in planta*, UAP56-mCherry and MOS11-eGFP-NLS fusion proteins were expressed in leaf cells of *N. benthamiana*, demonstrating that all fusion proteins localise to nuclei (Fig. S4). Analysis of the protein interactions using FRET-APB revealed significant FRET signals for MOS11 and MOS11 Δ NC, while only background levels were detected with MOS11 Δ α (Fig. 1b). Similarly, full-length MOS11 and MOS11 Δ NC interacted with GST-UAP56 in GST pull-down assays *in vitro*, while no interaction occurred with MOS11 Δ α (Fig. 1c). In conclusion, these assays demonstrate that the central helical part of MOS11 is crucial for the interaction with UAP56.

The binding affinity of MOS11 to a fluorescently labelled 25-nt ssRNA was examined using MST. Full-length MOS11 efficiently bound to the RNA (EC₅₀ = 432.6 ± 34.6 nM) (Fig. 1d) with an affinity in the range observed for other *Arabidopsis* export factors such as ALY1 and UIEF1 (Pfaff *et al.*, 2018;

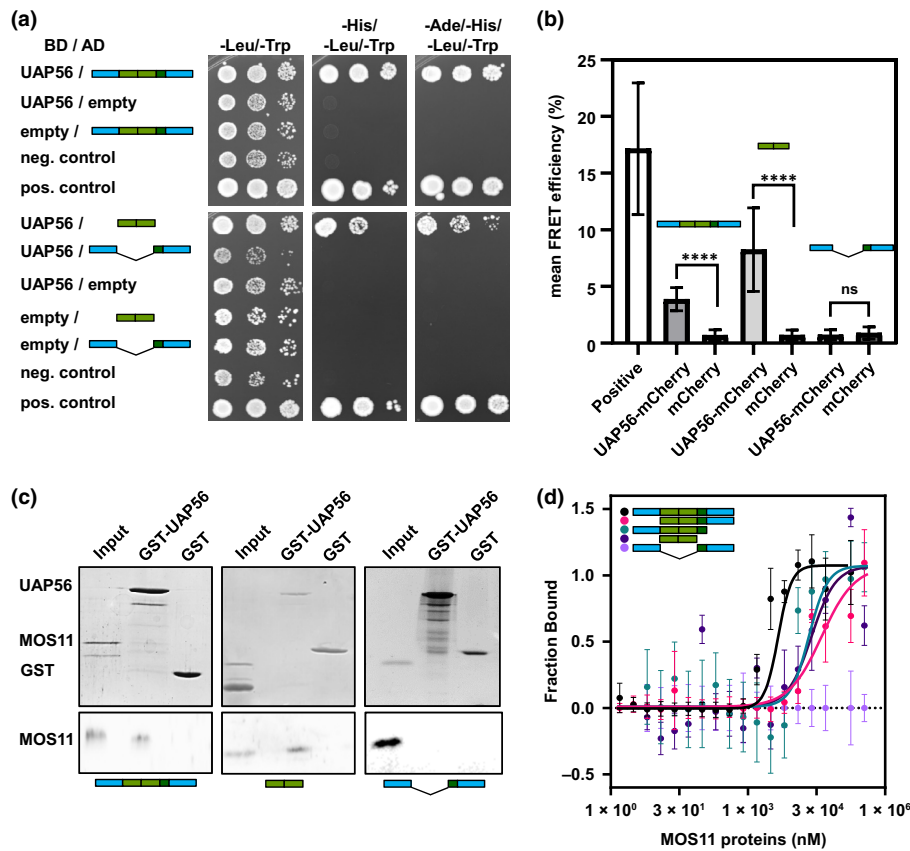


Fig. 1 Central α -helical region of MOS11 is required for interaction with UAP56 and RNA. (a) Yeast two-hybrid assays with cells harbouring as indicated UAP56-BD and MOS11-AD constructs grown on double, triple or quadruple drop-out medium. (b) Protein interactions analysed by FRET-ABP. *Nicotiana benthamiana* leaves were co-infiltrated with vectors directing the expression of the indicated donor (eGFP, MOS11) – acceptor (mCherry, UAP56) combinations as well as of positive and negative controls. Transiently transformed cells were analysed in two biological replicates by acceptor photobleaching forster resonance energy transfer (FRET). Mean FRET-APB efficiencies (\pm SD, 8 analysed nuclei each) are shown, which were analysed using Student's *t*-test ($P < 0.001$). (c) Glutathione S transferase (GST) pull-down experiments with UAP56-GST and the indicated 6xHis-tagged MOS11 proteins. Proteins eluted from GST-UAP56 or from GST were analysed by SDS-PAGE in combination with Coomassie staining (top) and Western blot (bottom) using an antibody directed against the 6xHis-tag. Aliquots (10%) of the protein input are shown. (d) RNA-binding of full-length and truncated MOS11 proteins analysed by MicroScale Thermophoresis. Increasing concentrations of the indicated MOS11 proteins were incubated with a Cy3-labelled 25-nt RNA oligonucleotide (5'-AAAACAAAUAGCACCGUAAAGCAC) and binding was fitted using Hill equation to determine EC₅₀ values. Data represent the mean \pm SD of at least three biological with three technical replicates. ****, $P \leq 0.0001$.

Ehrnsberger *et al.*, 2019b). Deletion of both the N-terminal or C-terminal region severely reduced the affinity for RNA, indicating decreased binding only at higher concentrations (calculated to be 6513 ± 245.1 and 4890 ± 355.2 nM, for MOS11 Δ N and MOS11 Δ C, respectively). The individual central helical domain bound to RNA with clearly lower affinity (1882 ± 108.2 nM) than full-length MOS11, whereas for MOS11 Δ α , no RNA-binding was detected (Fig. 1d). Therefore, the central α -helical domain is required for the RNA-binding of MOS11, but both the N- and C-terminal regions have a marked positive effect on the RNA interaction.

MOS11 and ALY1 can form a complex with UAP56, stimulating its enzymatic activities

The interaction between MOS11 and ALY1-4 with *Arabidopsis* UAP56 was demonstrated *in vitro* and *in vivo* by pull-down and

yeast two-hybrid assays as well as FRET measurements in plant cells (Kammel *et al.*, 2013; Sørensen *et al.*, 2017; Pfaff *et al.*, 2018). Consistently, these proteins co-purified with TREX components, when isolated from *Arabidopsis* cells by affinity chromatography (Sørensen *et al.*, 2017). However, from these analyses, it could be not elucidated, whether MOS11 and ALY proteins simultaneously can interact with UAP56, which we addressed using a three-component binding assay. To this end, GST-ALY1 was immobilised on glutathione sepharose beads. Added 6xHis-MOS11 (in contrast to 6xHis-UAP56) did not bind to ALY1 and thus could not be co-eluted from the beads (Fig. 2a). However, when 6xHis-UAP56 and 6xHis-MOS11 together were added to GST-ALY1, both 6xHis-UAP56 and 6xHis-MOS11 co-eluted from the beads. Neither 6xHis-UAP56 nor 6xHis-MOS11 interacted in this assay with unfused GST (Fig. 2a). This suggests that MOS11 and ALY1 together can interact with UAP56, as observed for the human orthologues (Dufu *et al.*, 2010).

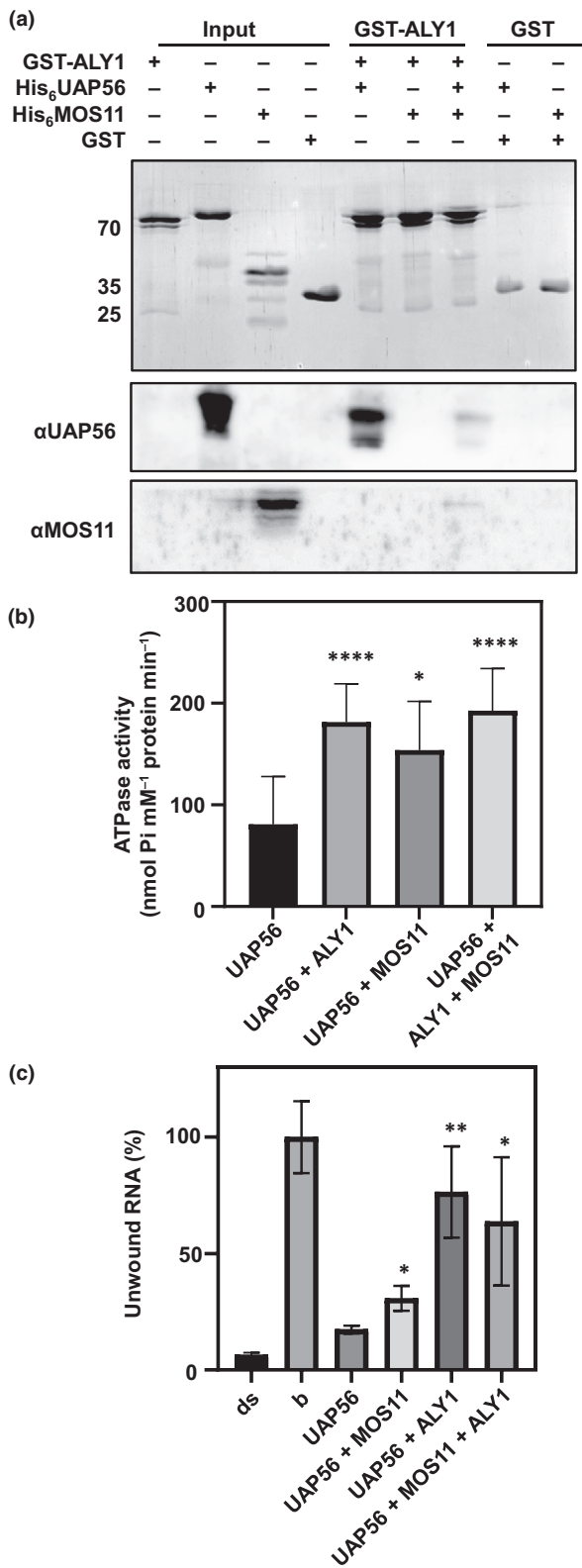


Fig. 2 MOS11 and ALY1 interact with UAP56, and stimulate its ATPase and helicase activities. (a) Glutathione S transferase pull-down assay illustrating that UAP56 can simultaneously interact with MOS11 and ALY1. UAP56 interacts with GST-ALY1, but association with MOS11 requires the presence of UAP56. Input samples and proteins eluted from the glutathione beads were analysed by SDS-PAGE (top panel) and immunoblotting using an antibody against the 6xHis-tag (bottom panels). Numbers on the left indicate the migration position of molecular weight markers (kDa). (b) The ATPase activity of UAP56 is stimulated by the addition of ALY1 and/or MOS11. Average values from three independent biological and three technical assays are shown and error bars represent the standard deviation. (c) The helicase activity of UAP56 is enhanced by the addition of ALY1 and/or MOS11. dsRNA untreated (ds) or boiled (b) served as references in the relative dsRNA unwinding assay. Average values of three replicate assays are shown and asterisks indicate statistical significance according to Student's *t*-test (*, $P \leq 0.05$; **, $P \leq 0.01$; ***, $P \leq 0.0001$) in b, c.

Arabidopsis UAP56 with ATP resulted in ATP-hydrolysis (Kammel *et al.*, 2013), while in the presence of ALY1, MOS11 or ALY1/MOS11 only low levels of ATP-hydrolysis were observed (Fig. S5a). Incubation of UAP56 along with ALY1 or MOS11 or with both proteins similarly increased the ATPase activity approximately twofold (Fig. 2b). In addition to its ATPase activity, *Arabidopsis* UAP56 was shown to have ATP-dependent RNA helicase activity (Kammel *et al.*, 2013). The helicase activity was examined using a dsRNA unwinding assay and boiling of the dsRNA served as a control for the strand separation (Fig. S5b,c). No obvious RNA unwinding activity could be demonstrated for MOS11, ALY1 and ALY1/MOS11 in the absence of UAP56 (Fig. S5b). Compared with incubation of the dsRNA with UAP56 alone, the addition of MOS11 slightly increased the unwinding activity of UAP56 (Figs 2c, S5c). Incubation of UAP56 together with ALY1 or with ALY1 and MOS11 similarly enhanced the unwinding activity of UAP56 approximately threefold. Taken together, ALY1 and MOS11 can stimulate the *in vitro* ATPase and RNA helicase activities of UAP56, but simultaneous addition of both proteins does not exceed the effect of the proteins added individually.

MOS11 and ALYs synergistically influence vegetative and reproductive development as well as mRNA export

The absence of MOS11 caused only mild effects on growth and development of *Arabidopsis* plants (Germain *et al.*, 2010). Similarly, double mutants defective in ALY1 and ALY2 or in ALY3 and ALY4 phenotypically resemble WT plants (Pfaff *et al.*, 2018). To examine the consequences of simultaneous loss of MOS11 in combination with ALYs, we generated *mos11 aly1 aly2* and *mos11 aly3 aly4* triple mutants by genetic crossing. In the course of these experiments, we realised that we were unable to generate plants homozygous for all three mutations. However, we obtained plants homozygous for two mutant loci and heterozygous for one of the *aly* mutations with the genotypes *mos11^{-/-} aly1^{-/-} aly2^{+/+}* (termed in the following *mos11 aly1/2*) and *mos11^{-/-} aly3^{-/-} aly4^{+/-}* (termed *mos11 aly3/4*) that we analysed in more detail. Consistent with earlier studies (Germain *et al.*, 2010; Pfaff *et al.*, 2018), *mos11* single-mutant as well as *aly1/2* and *aly3/4* double-mutant plants are phenotypically only

Subsequently, we tested whether the interaction between MOS11 and ALY1 with UAP56 influences the enzymatic activities of the RNA helicase. First, the ATPase activity of UAP56 was analysed. As previously demonstrated, incubation of

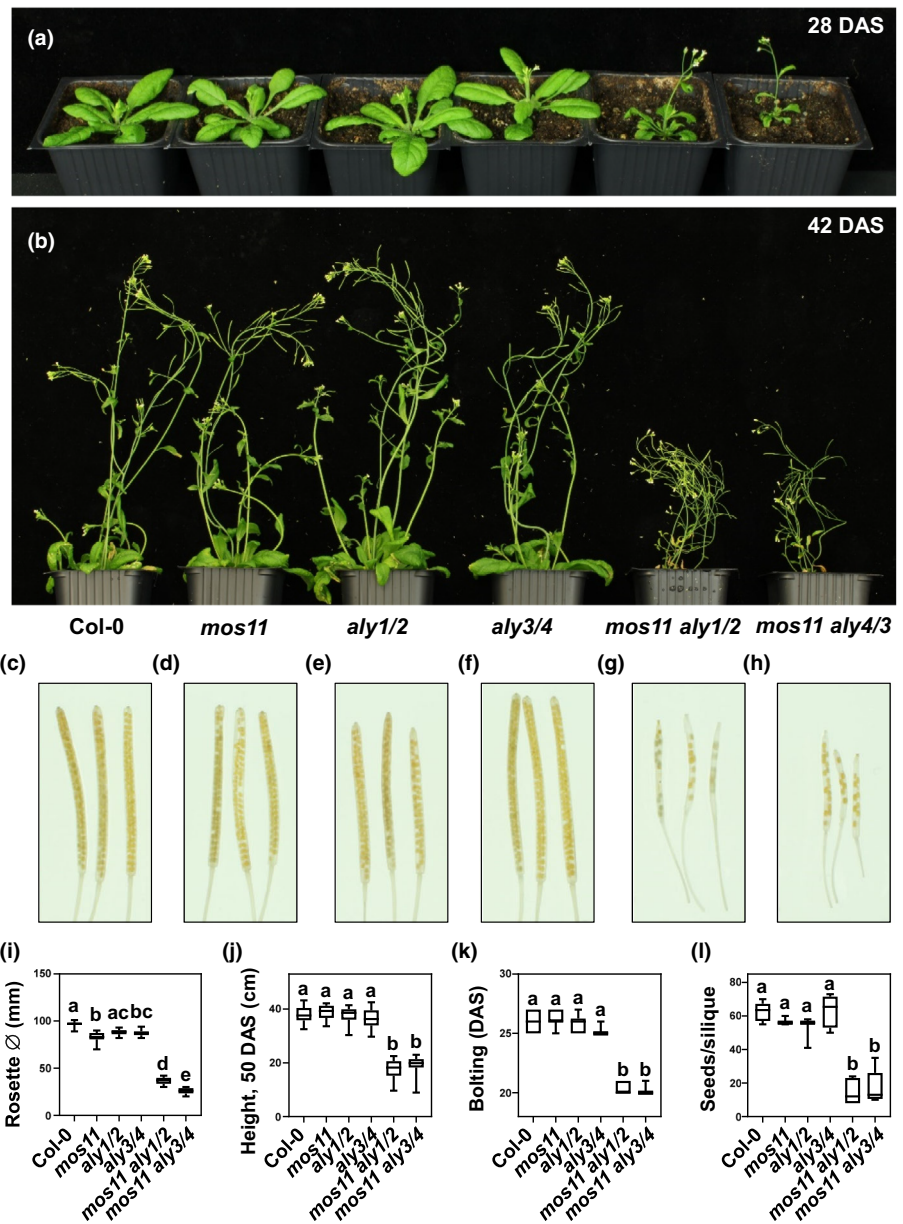


Fig. 3 *Arabidopsis thaliana* plants deficient in MOS11 and ALYs exhibit severe vegetative and reproductive defects. In the course of generating triple mutants lacking MOS11 in combination with ALY1/2 and in combination with ALY3/4 revealed that no triple homozygous plants could be obtained. Therefore, plants homozygous for two mutant loci and heterozygous for one of the *aly* mutations with the genotypes *mos11^{-/-}aly1^{-/-}aly2^{-/+}* (termed *mos11 aly1/2*) and *mos11^{-/-}aly3^{-/+}aly4^{-/-}* (termed *mos11 aly3/4*) were analysed. (a, b) Phenotype of the triple mutants, the parental lines and Col-0 wild-type documented at 28 and 42 d after stratification. (c–h) Cleared siliques illustrating the seed set of the genotypes depicted in the same order as in (a, b). (i–l) Quantification of selected phenotypic features. Error bars indicate SD of 15 plants. Data sets marked with different letters are significantly different as assessed by a multicomparison Tukey’s test ($P < 0.05$) after one-way analysis of variance.

mildly affected including rosette diameter, plant height, bolting time and seed set (Fig. 3). Likewise, the size and shape of leaves resembles that of Col-0 WT plants (Fig. S6). In contrast to that, the phenotype of *mos11 aly1/2* and *mos11 aly3/4* plants differs strikingly from Col-0 and the parental lines. Thus, the triple mutants exhibit a decreased rosette diameter (Fig. 3a,i) with smaller leaves (Fig. S6), reduced height (Fig. 3b,j), early bolting (Fig. 3a,k) and reduced seed set (Fig. 3c–h,l).

In view of the severely affected phenotypes of the *mos11 aly1/2* and *mos11 aly3/4* plants, we examined them for possible mRNA export defects using whole mount *in situ* hybridisation with a fluorescently labelled oligo(dT) probe and confocal laser scanning microscopy. For comparison, Col-0 plants were analysed and the quadruple *4xaly* mutant that exhibited a severe mRNA export defect as demonstrated using this *in situ* hybridisation assay (Pfaff *et al.*, 2018). Both *mos11 aly1/2* and *mos11 aly3/4* mutants

showed (relative to the cytosolic signal) a stronger nuclear fluorescence signal than that observed for Col-0 (Fig. 4), indicating mRNA export defects. Quantification of the fluorescent signals revealed that the impairment with the *mos11 aly1/2* and *mos11 aly3/4* mutants is even more prominent than with the *4xaly* mutants. Thus, while the *mos11* single-mutant exhibits only mild mRNA export defects (Sørensen *et al.*, 2017), the combined inactivation of MOS11 and ALY1/2 or ALY3/4 caused severe defects in vegetative and reproductive development as well as it resulted in a clearly negative impact on mRNA export.

MOS11 is required for nucleocytoplasmic transport of a subset of mRNAs

To identify mRNAs that are exported from the nucleus depended on MOS11, we intended to sequence mRNAs of nuclear and

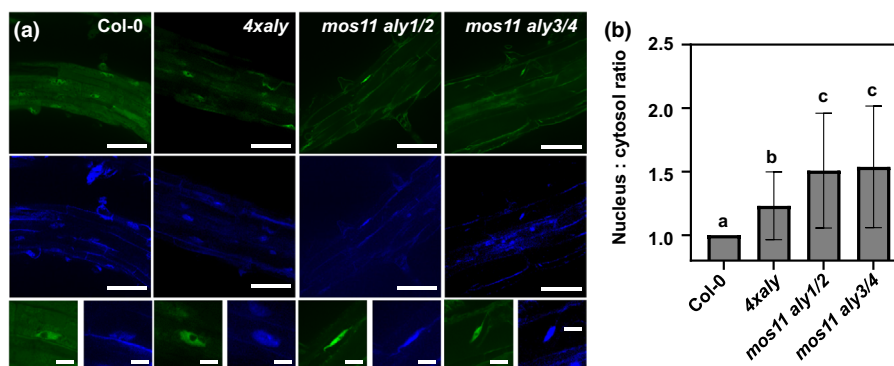


Fig. 4 Plants deficient in MOS11 and ALYs are impaired in mRNA export. Plants of the indicated genotypes were analysed by whole mount *in situ* hybridization with a fluorescently labelled oligo(dT) probe was performed in roots from 14 d after stratification seedlings. (a) Confocal laser scanning microscopy images of representative sections of roots of the indicated genotypes with an Alexa Fluor 488 oligo (dT) signal (green) and the corresponding DAPI signal (blue). Bars: 60 μ m (top rows) and 20 μ m (bottom row). (b) Average nuclear/cytoplasmic Alexa Fluor 488 signal ratio of ≥ 60 nuclei per genotype. The ratios are shown relative to Col-0 (ratio of 1), with error bars indicating SD. Data sets marked with different letters are significantly different as assessed by a multicomparison Tukey's test ($P < 0.05$) after one-way analysis of variance.

cytoplasmic fractions isolated from *mos11* and Col-0 plants. Nuclear and cytoplasmic fractions prepared from plants 14 d after stratification were assessed by immunoblotting with antibodies against histone H3 (nuclear marker) and UDP-glucose pyrophosphorylase (UGPase, cytoplasmic marker). The immunoblot analysis revealed that α -H3 and α -UGPase reacted essentially with proteins of the nuclear and cytoplasmic fractions, respectively, illustrating the quality of the cell fractionation (Fig. S7a).

RNA isolated from the nuclear and cytoplasmic fractions was examined by high-throughput sequencing (RNA-seq) to determine genotype-dependent changes in mRNA distribution. Principal component analysis of the RNA-seq data demonstrated that the replicates of each subcellular fraction and genotype grouped distinctly (Fig. S7b).

We expected that export defects of transcripts would be manifested by enrichment in the nuclear fraction and simultaneous depletion of the transcripts in the cytoplasmic fraction in *mos11* compared with Col-0. Therefore, we designed a statistical test to directly assess the changes in the nuclear and cytosolic transcript abundance ratio compared with Col-0. Our analysis revealed 611 differentially distributed transcripts (FDR of 5%, Table S3), which can be grouped into two clusters (Fig. 5a). Genes in Cluster 1 (termed Cyt enriched, $n = 315$) showed a decrease in the proportion of nuclear transcripts and a concomitant increase in cytosolic transcripts. Cluster 2 (termed Nuc enriched, $n = 296$) showed the opposite distribution to Cluster 1, conforming to the expected feature of transcripts defective in export in *mos11*. Gene ontology (GO) analysis of these differentially enriched transcripts revealed that the GO terms 'metabolic process' and 'response to stimulus' were prominent among the transcripts enriched in nuclei of *mos11* plants grown under standard conditions (Fig. 5b). In the category 'response to stimulus', examples related to 'light intensity', 'decreased oxygen levels' and 'response to cold' were found (Fig. 5c), while mainly photosynthesis-related transcripts comprised those of the category 'metabolic process' (Fig. S8). Subsequently, various molecular characteristics of the differentially enriched transcripts were explored. Transcripts

enriched in nuclei of *mos11* relative to Col-0 turned out to be shorter (median 1314 bp) than transcripts enriched in the cytoplasm (median 2899 bp) or unaffected transcripts (median of 1874 bp) (Fig. 5d). In addition, the coding sequences (CDSs) of nuclear enriched transcripts have a higher GC-content (median 46.5%) than those of other transcripts (median of 44.7%), and the GC-content of the UTRs hardly differs between those transcript categories (Fig. 5e–g). Since the export of GC-rich transcripts appears to be particularly affected in *mos11* plants, we tested whether MOS11 interacts differently with GC-rich relative to AU-rich RNA. Using MST, the affinity of MOS11 for GC-rich and AU-rich RNA oligonucleotides was determined revealing that the protein bound with clearly higher affinity to the GC-probe (56.4 ± 17.8 nM) when compared to the AU-probe (2277.3 ± 196.9 nM; Fig. S9a). UAP56 was analysed for comparison, demonstrating that it bound similarly to both probes (4401 ± 654.6 nM and 6467 ± 720.3 nM, for the GC and AU probes, respectively; Fig. S9b).

MOS11 promotes efficient response to environmental conditions

In view of the mild phenotype of *mos11* plants and the prominent enrichment of stimulus responsive genes among those differentially affected in *mos11* plants, we considered analysing the performance of *mos11* plants under adverse conditions. Since we have recent data sets, determining the transcriptomic changes induced by exposure of *Arabidopsis* plants to 100 mM NaCl or to heat treatment at 37°C (Obermeyer *et al.*, 2022, 2023), we analysed the molecular features of the transcripts upregulated under these conditions. Interestingly, the transcripts upregulated under these stress conditions proved to be shorter with more GC-rich CDSs than unaffected transcripts (Fig. S10a, b). Therefore, the transcripts upregulated by elevated NaCl concentration and HS share features with transcripts enriched in nuclei of *mos11* plants. To test whether *mos11* plants are affected by elevated NaCl concentrations, *mos11* mutant plants along

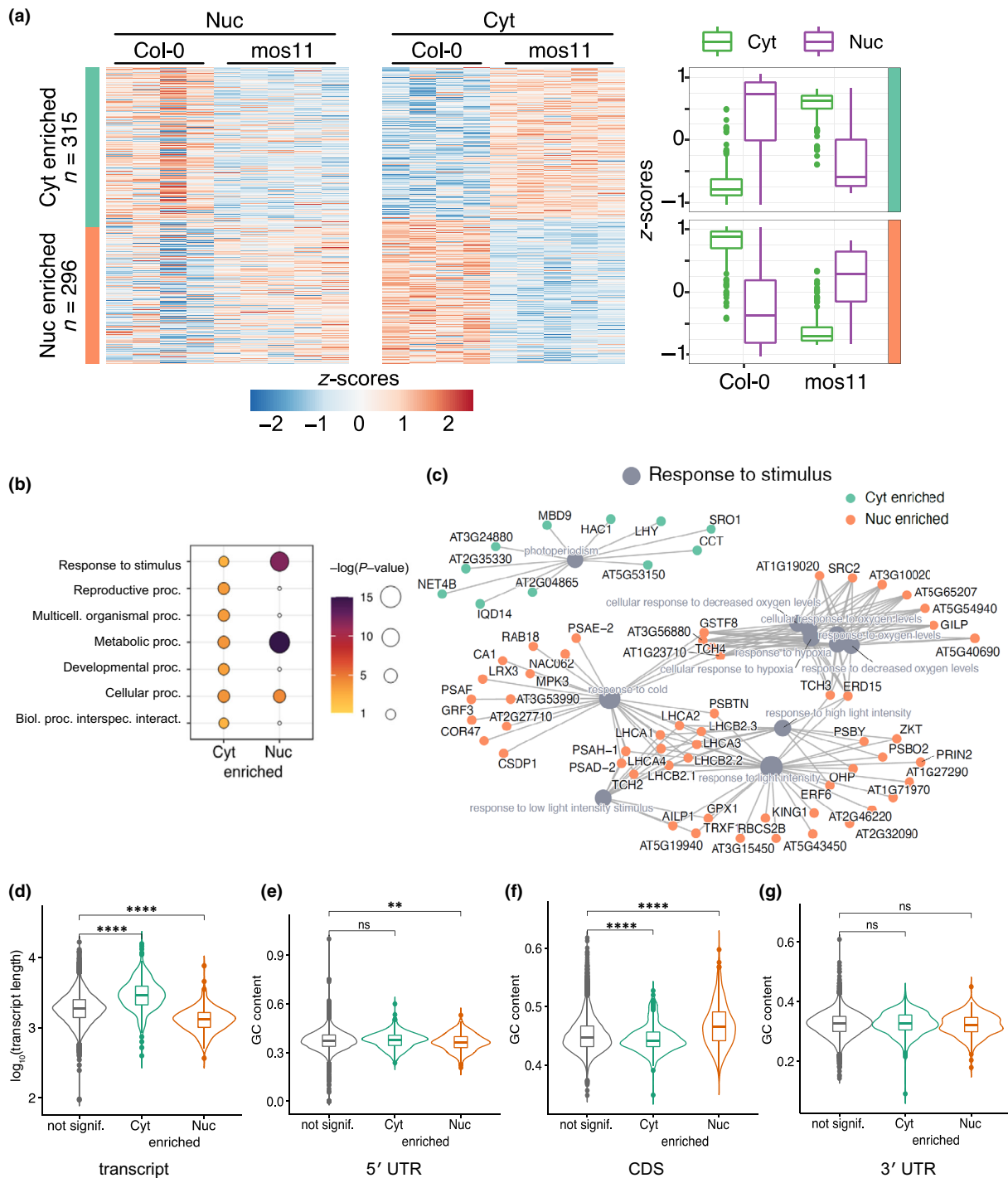


Fig. 5 In *mos11* plants, the mRNA export of a subset of transcripts is impaired that exhibits shorter transcript length and increased GC-content. (a) Transcripts that compared to Col-0 (based on RNA-seq analysis) show a different nuclear/cytoplasmic abundance (left panels) can be grouped into Cluster 1 (Cyt enriched) and Cluster 2 (Nuc enriched) using k-means clustering. The abundance of these transcripts is inversely correlated (right panel). Here, the box represents the interquartile range (IQR). The line inside the box represents the median of the dataset. The whiskers extend from the edges of the box to the first and third quartiles, but no further than 1.5 times of the IQR. Any data points outside this range are plotted individually as dots. (b) Functional annotation of nuclear enriched transcripts demonstrated an enrichment of the Gene Ontology terms 'metabolic processes' and 'response to stimulus'. (c) Under our normal growth conditions, subterms such as response to cold and light are enriched within the parent term 'response to stimulus'. (d) Transcripts enriched in nuclei of *mos11* relative to Col-0 are shorter than unaffected transcripts. (e–g) Coding sequences of nuclear enriched transcripts have a higher GC-content. Violin plots show the kernel probability density of the data. The box represents the interquartile range (IQR). The line inside the box represents the median of the data set. The whiskers extend from the edges of the box to the first and third quartiles, but no further than 1.5 times of the IQR. Any data points outside this range are plotted individually as dots. Unpaired *t*-test was used for statistical analysis (**, $P \leq 0.01$; ****, $P \leq 0.0001$; ns, not significant).

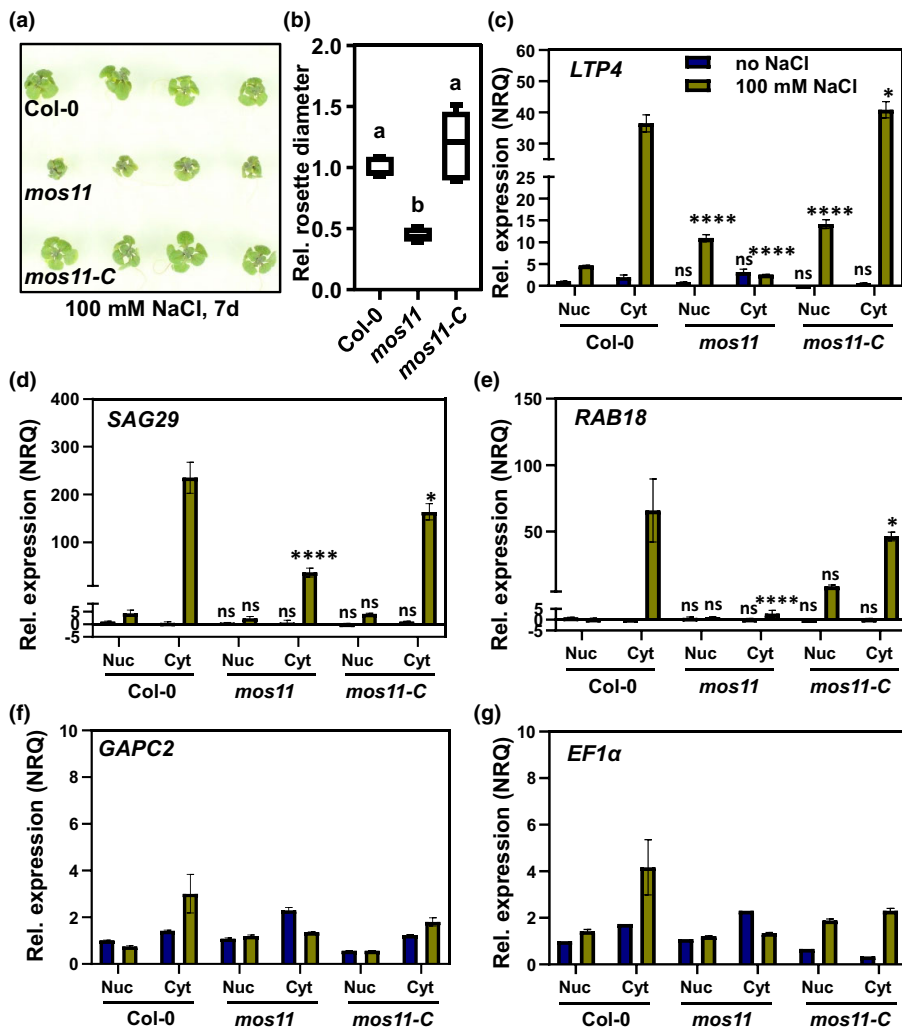


Fig. 6 Export of mRNAs upregulated upon exposure to elevated NaCl concentrations is impaired in *mos11* plants. (a) Phenotype of *Arabidopsis* Col-0, *mos11* and *mos11-C* complementation plants grown on Murashige and Skoog (MS) medium for 7d and then for 7d on MS containing 100 mM NaCl. (b) Quantification of the rosette diameter relative to Col-0 of 15 plants ($n = 3$). Differences in rosette diameter between genotypes are indicated by different letters as assessed by a multicomparison Tukey's t -test ($P < 0.05$) after one-way analysis of variance. (c–g) The relative abundance of selected mRNAs for the nuclear and cytoplasmic fraction of the three genotypes by RT-qPCR. *LTP4*, *SAG29* and *RAB18* (c–e) are genes that are upregulated upon exposure to 100 mM NaCl, while the housekeeping genes *GAPC2* and *EF1 α* (f, g) served as references. The relative normalised quantities (NRQ) were calculated and normalised to housekeeping genes. Significant differences (indicated by asterisks) were determined relative to Col-0 using two-way ANOVA followed by Tukey's comparisons test (*, $P \leq 0.05$; ****, $P \leq 0.0001$; ns, not significant). Error bars represent SD of three biological replicates each performed in two technical replicates.

with Col-0 WT and *mos11* harbouring a complementation construct (expressing MOS11 fused to RFP under control of the *MOS11* promoter (Sørensen *et al.*, 2017), termed *mos11-C*) were grown on MS medium supplemented with 100 mM NaCl. Compared with Col-0 and *mos11-C*, the growth of *mos11* plants was clearly reduced in the presence of 100 mM NaCl, which is also evident from the decreased rosette diameter (Fig. 6a,b). To explore, whether transcripts of NaCl-regulated genes are differentially exported in the three genotypes, nuclear and cytoplasmic RNA was isolated from *mos11*, Col-0 and *mos11-C* after 3 h exposure to 100 mM NaCl or without. Three genes that are upregulated upon 3-h exposure to 100 NaCl in Col-0 (*LTP4*, *SAG29*, *RAB18* (Obermeyer *et al.*, 2022)) were selected for analysing transcript abundance by quantitative reverse transcription polymerase chain reaction. Two housekeeping genes (*EF1 α* , *GAPC2*) were examined for comparison. Expression level and export of *LTP4*, *SAG29* and *RAB18* mRNAs in Col-0 was significantly increased after exposure to NaCl (Fig. 6c–e). For *mos11* plants, substantially lower levels of the three transcripts were detected in the cytoplasm after NaCl treatment. In *mos11-C*, the distribution of these mRNAs resembled that observed in Col-0. Expression and distribution of *EF1 α* and *GAPC2* mRNAs was

not markedly affected by genotype and NaCl treatment (Fig. 6f, g). This suggests that MOS11 is required for proper export of mRNAs that are upregulated by NaCl exposure.

In addition, we investigated with *mos11* plants the consequences of heat exposure. Treatment of *mos11* with HS of 37°C for 48 h resulted in lethality of *c.* 90% of the plants, whereas *c.* 90% of Col-0 and *mos11-C* plants recovered from the HS (Fig. 7a,b). To evaluate the possible effects on mRNA distribution, nuclear and cytoplasmic RNA was isolated from *mos11*, Col-0 and *mos11-C* after 3-h exposure to HS of 37°C or without. Transcript abundance was determined by quantitative reverse transcription polymerase chain reaction for four genes that are upregulated upon 3-h exposure to HS of 37°C for 3 h in Col-0 (*HSP101*, *HSP70*, *HSP18.2*, *HSP17.6B* (Obermeyer *et al.*, 2023)). Two housekeeping genes (*EF1 α* , *GAPC2*) were examined for comparison. A massive upregulation of the four HS-induced genes was observed for all genotypes (Fig. 7c,d). Strikingly, when compared to Col-0, in *mos11* plants, a significantly lower portion of the transcripts was detected in the cytoplasm. In *mos11-C*, the distribution of these mRNAs resembled that observed in Col-0. Expression and distribution of the mRNAs of the two housekeeping genes differed hardly between

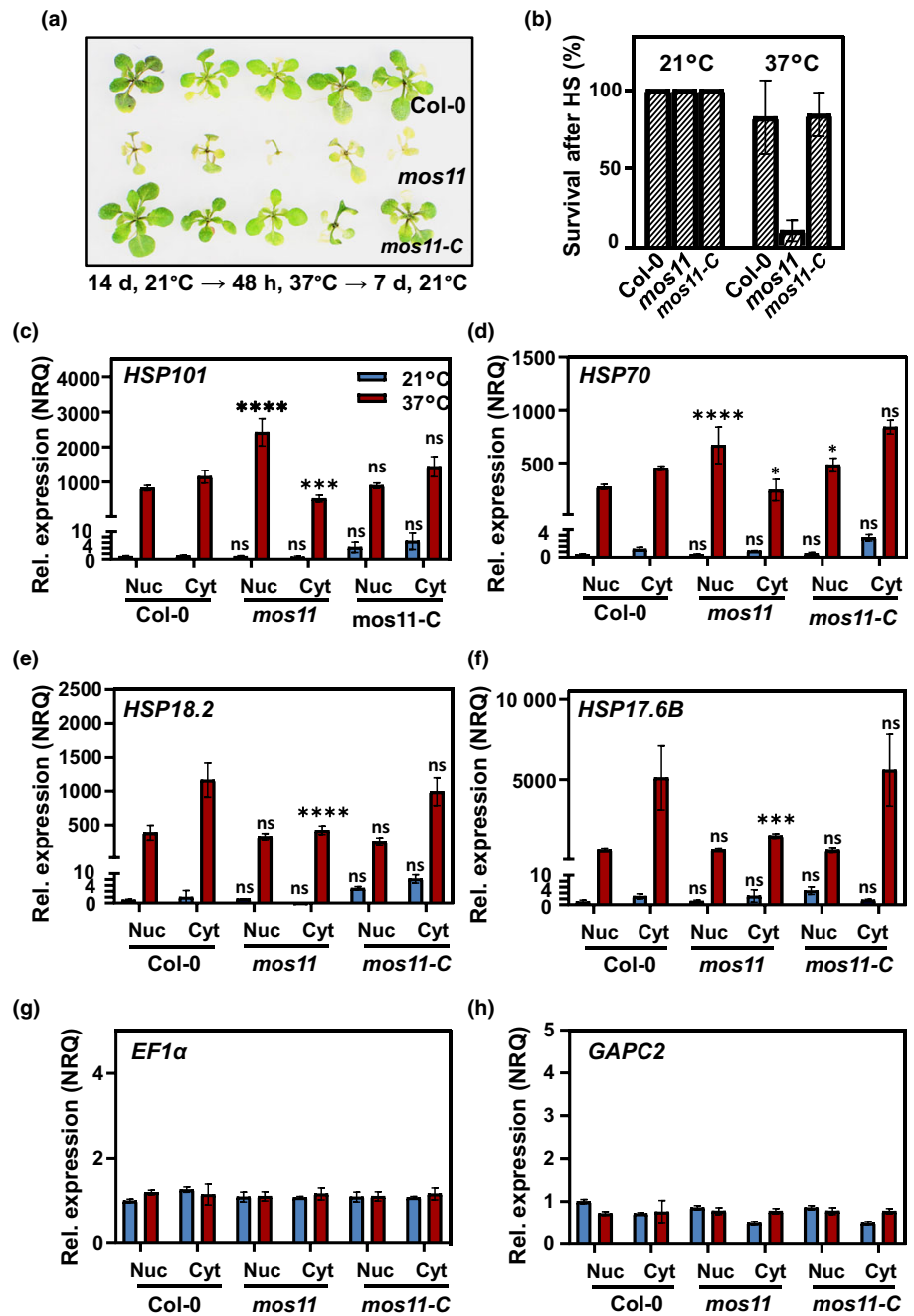


Fig. 7 Export of mRNAs upregulated upon exposure to HS at 37°C is impaired in *mos11* plants. (a) Phenotype of *Arabidopsis* Col-0, *mos11* and *mos11-C* complementation plants grown on Murashige and Skoog medium according to the indicated temperature scheme were documented after the final 7-d recovery period. (b) Survival rate of the different genotypes without heat stress (HS; 21°C) or after 48-h HS (37°C). Error bars indicate standard deviation of 15 plants ($n = 3$). (c–h) The relative abundance of selected mRNAs was determined following cell fractionation for the nuclear and cytoplasmic fraction of the three genotypes by reverse transcription quantitative polymerase chain reaction. *HSP101*, *HSP70*, *HSP18.2* and *HSP17.6B* (c–f) are genes that are upregulated upon exposure to HS at 37°C for 3 h, while the housekeeping genes *GAPC2* and *EF1α* (g, h) served as references. The relative normalised quantities were calculated and normalised to housekeeping genes. Significant differences (indicated by asterisks) were determined relative to Col-0 using two-way ANOVA followed by Tukey's multiple comparisons test (*, $P \leq 0.05$; ***, $P \leq 0.001$; ****, $P \leq 0.0001$; ns, not significant). Error bars represent SD of three biological replicates each performed in two technical replicates.

genotypes and treatment (Fig. 7g,h). These results indicate that the export factor MOS11 is required for efficient nucleocytoplasmic transport of mRNAs that are induced by HS.

Discussion

Export of mature mRNAs from the cell nucleus is intimately coupled to transcription and pre-mRNA processing, and the TREX complex plays a central role in the coordination of these processes (Maniatis & Reed, 2002; Moore & Proudfoot, 2009; Wickramasinghe & Laskey, 2015; Heath *et al.*, 2016). The yeast and mammalian MOS11 orthologs, Tho1 and CIP29/SARNP,

were identified as TREX components that exhibit RNA-binding activity. Both proteins bind ssRNA and for Tho1 the main RNA-binding activity resides within the C-terminal region of the protein following the SAP domain (Jimeno *et al.*, 2006; Sugiura *et al.*, 2007). In case of MOS11, the central α -helical domain is required for RNA-binding, but both the N- and C-terminal regions clearly enhance the affinity for RNA. In addition, our RNA-binding experiments demonstrated that compared with AU-rich RNA, MOS11 interacts preferentially with GC-rich RNA, while UAP56 bound similarly to both probes. The association between CIP29 and MOS11 with the TREX complex is mediated by direct interaction with the RNA helicase UAP56 (or

the mammalian paralog URH49) (Dufu *et al.*, 2010; Yamazaki *et al.*, 2010; Kammel *et al.*, 2013; Sørensen *et al.*, 2017). Using different assays, we have determined here that the central α -helical region of MOS11 is required for the interaction with UAP56 *in vitro* and *in vivo*. This is consistent with a very recent crystal structure of yeast Tho1 in complex with human UAP56 that demonstrated interaction of the Tho1 α -helices with UAP56 (Xie *et al.*, 2023). In line with an earlier study (Dufu *et al.*, 2010), structural information also indicated that ALY and Tho1/CIP29 can interact simultaneously with the N- and C-terminal domains of UAP56, respectively (Xie *et al.*, 2023). Similarly, *Arabidopsis* UAP56 bridged the interaction between MOS11 and ALY1 in GST pull-down assays. The addition of MOS11 or ALY1 enhanced the ATPase and RNA unwinding activities of UAP56, but the addition of both proteins had no additive effect. Stimulation of the ATPase and helicase activities of UAP56 was also observed for mammalian CIP29 and ALY proteins (Sugiura *et al.*, 2007; Chang *et al.*, 2013). Thus, MOS11 (together with ALYs) as well as its orthologs in other organisms may modulate the enzymatic activities of UAP56-type helicases to remodel mRNPs during maturation and nuclear export (Bourgeois *et al.*, 2016).

Yeast cells lacking THO1 have no apparent phenotype and grow with WT doubling time (Piruat & Aguilera, 1998). By contrast, yeast cells lacking Yra1 (ortholog of ALYs) are non-viable (Sträßer & Hurt, 2000). *Arabidopsis mos11* plants as well as *aly* single- and double-mutant plants are phenotypically only mildly affected (Germain *et al.*, 2010; Pfaff *et al.*, 2018). As both MOS11 and ALYs are RNA-binding proteins that interact directly with UAP56, we examined the consequences of a simultaneous loss of ALY1/2 or ALY3/4 in combination with MOS11 by generating the respective triple mutants. We were unable to generate plants homozygously mutated for three loci, but we could recover plants homozygous for two mutant loci and heterozygous for one of the *aly* mutations. These plants exhibit various defects in vegetative and reproductive development. Interestingly, the *mos11 aly1/2* and *mos11 aly3/4* triple mutants exhibit nuclear accumulation of mRNAs that is even more pronounced than that of the *4xaly* quadruple mutant lacking all four ALY proteins (Pfaff *et al.*, 2018). These results suggest a remarkable synergistic action of MOS11 and ALY mRNA export factors in *Arabidopsis*.

In plants, it is largely obscure to which extent mRNA export factors function generally in nucleocytoplasmic transport of transcripts or whether they influence only subsets of transcripts, although for *aly1* mutants reduced mRNA export affecting a portion of mRNAs was reported (Choudury *et al.*, 2019). To identify mRNAs that require MOS11 for efficient nucleocytoplasmic transport, Col-0 and *mos11* plants were comparatively analysed by cell fractionation coupled with RNA-seq. The set of mRNAs that were found to be enriched in the nuclei of *mos11* plants were shorter than non-affected transcripts and they exhibited a higher GC-content within the coding sequences. In human cells, GC-content correlates with cytosolic localisation of mRNAs (Mordstein *et al.*, 2020) and transcripts with higher GC-content preferentially require the TREX components UAP56 and ALY for nucleocytoplasmic transport (Zuckerman *et al.*, 2020). In line

with our findings, the subset of mRNAs that were dependent on CIP29/SARNP for export had a higher GC-content than mRNAs, whose export was not altered by the knockdown of CIP29/SARNP (Xie *et al.*, 2023). The higher affinity of MOS11 for GC-rich RNA, as determined by our MST measurements, suggests that the RNA-binding activity of MOS11 may influence the selection of mRNAs for export. However, some mRNAs were enriched in the cytoplasm of *mos11* plants and showed the opposite characteristics, being longer and having lower GC-content in the coding region as mRNAs enriched in the nucleus. We can only speculate about the causes of the cytoplasmic enrichment of these mRNAs. In view of the mild phenotype of *mos11* plants and the comparatively slight export defect, conceivably in the absence of MOS11 other export factors may take on its contribution in nucleocytoplasmic transport, resulting in altered composition of cytoplasmic mRNAs.

There is accumulating evidence that besides transcriptional reprogramming, plants make use of post-transcriptional regulation mediated by range of mRNA-binding proteins in response to biotic and abiotic stress, but it is unclear to which extent mRNA export is involved therein (Chinnusamy *et al.*, 2009; Parry, 2013; Staiger *et al.*, 2013; Yan *et al.*, 2022). Plants lacking MOS11 exhibit a clearly enhanced sensitivity to elevated concentrations of NaCl and to heat stress, suggesting that MOS11 is required for proper response to abiotic stress conditions, whereas MOS11 apparently is not involved in basal pathogen resistance (Germain *et al.*, 2010). The mRNAs enriched in nuclei of *mos11* plants under normal conditions are shorter with more GC-rich CDSs, characteristics that are shared by mRNAs upregulated in Col-0 by elevated NaCl concentrations and HS. Interestingly, under stress conditions, several such mRNAs were found to be less efficiently exported from the nuclei of *mos11* plants, when compared with Col-0. This indicates that MOS11 is required for efficient nucleocytoplasmic transport of subsets of mRNA that were upregulated upon treatment with elevated NaCl or by HS. Therefore, the function of MOS11 as mRNA export factor appears to be critical under abiotic stress conditions. This is in line with the role of the RNA helicase LOS4 in the response to altered ambient temperatures (Gong *et al.*, 2005) and the function of the THO subunit HPR1 in modulating aluminium resistance (Guo *et al.*, 2020).

Many export factors are recruited co-transcriptionally to mRNAs, which may be dependent on 5'-capping, splicing (exon junction complex) and/or 3'-end processing (Heath *et al.*, 2016; Ashkenazy-Titelman *et al.*, 2020). Consequently, various export factors including TREX are positioned along the mRNA in yeast and metazoa, finally licensing it for nucleocytoplasmic transport through nuclear pore complexes (Zenklusen *et al.*, 2002; Gromadzka *et al.*, 2016; Shi *et al.*, 2017; Fan *et al.*, 2019; Vipha-kone *et al.*, 2019). Recent biochemical and structural analyses of yeast and human mRNPs associated with TREX and export factors revealed that they are compact particles that contain multiple copies of TREX and ALY (Yra1 in yeast) (Bonneau *et al.*, 2023; Pacheco-Fiallos *et al.*, 2023). The co-transcriptional packaging of mRNAs appears to be a prerequisite for proper export of the transcripts and TREX in combination with ALY plays an essential

role in this process (Bonneau *et al.*, 2023; Pacheco-Fiallos *et al.*, 2023). In addition, CIP29/SARNP that can bind simultaneously with ALY to UAP56 may contribute to mRNP assembly (Xie *et al.*, 2023). Our finding that in *Arabidopsis* the concomitant loss of MOS11 and ALYs results in severe growth and mRNA export defects points to a scenario, in which the two types of factors collaborate in the export of a subset of mRNAs. The fact that in the *mos11* single mutant only a portion of mRNAs is enriched in the nucleus together with the preference of MOS11 for GC-rich RNA suggests a role for MOS11 in the selection of certain transcripts, which evidently is particularly relevant under abiotic stress conditions. It also illustrates that beyond transcriptional reprogramming, adjustable mRNA export is a critical tool in plant stress responses.

Acknowledgements

We would like to thank Klaus-Jürgen Tiefenbach and Reinhard Sterner for providing access to the CD spectrometer and help with the CD measurements, Zolile Morokane for contributions to the characterisation of plant lines and the Nottingham Arabidopsis Stock Centre (NASC) for providing Arabidopsis T-DNA insertion lines. This research was supported by the German Research Foundation (DFG) through grant SFB960/A6 to KDG. Open Access funding enabled and organized by Projekt DEAL.

Competing interests

None declared.

Author contributions

AR, IW and ST performed experiments. AR, IW, ST, US, GL and CM analysed data. MG and KDG designed the research, supervised the project and KDG wrote the manuscript. All authors discussed the results, commented on the manuscript and approved the final version.

ORCID

Klaus D. Grasser  <https://orcid.org/0000-0002-7080-5520>

Data availability

Code used to analyse the RNA-seq data and corresponding next-flow workflows are deposited at GitHub ([uschwartz/mos11](https://github.com/uschwartz/mos11)). Data sets produced in this study are available at Gene Expression Omnibus under accession GSE247811.

References

- Antosz W, Deforges J, Begcy K, Bruckmann A, Poirier Y, Dresselhaus T, Grasser KD. 2020. Critical role of transcript cleavage in Arabidopsis RNA polymerase II transcriptional elongation. *Plant Cell* 32: 1449–1463.
- Aravind L, Koonin EV. 2000. SAP – a putative DNA-binding motif involved in chromosomal organization. *Trends in Biochemical Sciences* 25: 112–114.
- Ashkenazy-Titelman A, Shav-Tal Y, Kehlenbach RH. 2020. Into the basket and beyond: the journey of mRNA through the nuclear pore complex. *The Biochemical Journal* 477: 23–44.
- Bonneau F, Basquin J, Steigenberger B, Schäfer T, Schäfer IB, Conti E. 2023. Nuclear mRNPs are compact particles packaged with a network of proteins promoting RNA-RNA interactions. *Genes & Development* 37: 505–517.
- Bourgeois CF, Mortreux F, Auboeuf D. 2016. The multiple functions of RNA helicases as drivers and regulators of gene expression. *Nature Reviews. Molecular Cell Biology* 17: 426–438.
- Chang CT, Hautbergue GM, Walsh MJ, Viphakone N, van Dijk TB, Philipsen S, Wilson SA. 2013. Chtop is a component of the dynamic TREX mRNA export complex. *EMBO Journal* 32: 473–486.
- Chinnusamy V, Gong Z, Zhu JK. 2009. Nuclear RNA export and its importance in abiotic stress responses of plants. *Current Topics in Microbiology and Immunology* 326: 235–255.
- Choudury SG, Shahid S, Cuerda-Gil D, Panda K, Cullen A, Ashraf Q, Sigman MJ, McCue AD, Slotkin RK. 2019. The RNA export factor ALY1 enables genome-wide RNA-directed DNA methylation. *Plant Cell* 31: 759–774.
- Darnell JE. 2013. Reflections on the history of pre-mRNA processing and highlights of current knowledge: a unified picture. *RNA* 19: 443–460.
- Dufu K, Livingstone MJ, Seebacher J, Gygi SP, Wilson SA, Reed R. 2010. ATP is required for interactions between UAP56 and two conserved mRNA export proteins, Aly and CIP29, to assemble the TREX complex. *Genes & Development* 24: 2043–2053.
- Ehrensberger HF, Grasser M, Grasser KD. 2019a. Nucleocytoplasmic mRNA transport in plants: export factors and their influence in growth and development. *Journal of Experimental Botany* 70: 3757–3763.
- Ehrensberger HF, Pfaff C, Hachani I, Flores-Tornero M, Sørensen BB, Längst G, Sprunck S, Grasser M, Grasser KD. 2019b. The UAP56-interacting export factors UIEF1 and UIEF2 function in mRNA export. *Plant Physiology* 179: 1525–1536.
- Ewels P, Magnusson M, Lundin S, Käller M. 2016. MultiQC: summarize analysis results for multiple tools and samples in a single report. *Bioinformatics* 32: 3047–3048.
- Fan J, Wang K, Du X, Wang J, Chen S, Wang Y, Shi M, Zhang L, Wu X, Zheng D *et al.* 2019. ALYREF links 3'-end processing to nuclear export of non-polyadenylated mRNAs. *EMBO Journal* 38: e99910.
- Gaouar O, Germain H. 2013. mRNA export: threading the needle. *Frontiers in Plant Science* 4: 59.
- Germain H, Qu N, Cheng YT, Lee E, Huang Y, Dong OX, Gannon P, Huang S, Ding P, Li Y *et al.* 2010. MOS11: a new component in the mRNA export pathway. *PLoS Genetics* 6: e1001250.
- Gong Z, Dong CH, Lee H, Zhu J, Xiong L, Gong D, Stevenson B, Zhu JK. 2005. A DEAD box RNA helicase is essential for mRNA export and important for development and stress responses in *Arabidopsis*. *Plant Cell* 17: 256–267.
- Gromadzka AM, Steckelberg AL, Singh KK, Hofmann K, Gehring NH. 2016. A short conserved motif in ALYREF directs cap- and EJC-dependent assembly of export complexes on spliced mRNAs. *Nucleic Acids Research* 44: 2348–2361.
- Guo J, Zhang Y, Gao H, Li S, Wang Z-Y, Huang C-F. 2020. Mutation of HPR1 encoding a component of the THO/TREX complex reduces STOP1 accumulation and aluminium resistance in *Arabidopsis thaliana*. *New Phytologist* 228: 179–193.
- Heath CG, Viphakone N, Wilson SA. 2016. The role of TREX in gene expression and disease. *The Biochemical Journal* 473: 2911–2935.
- Howe KJ. 2002. RNA polymerase II conducts a symphony of pre-mRNA processing activities. *Biochimica et Biophysica Acta* 1577: 308–324.
- Jacobsen JOB, Allen MD, Freund SMV, Bycroft M. 2016. High-resolution NMR structures of the domains of *Saccharomyces cerevisiae* Tho1. *Acta Crystallographica. Section F, Structural Biology Communications* 72: 500–506.
- Jiang L, Schlesinger F, Davis CA, Zhang Y, Li R, Salit M, Gingeras TR, Oliver B. 2011. Synthetic spike-in standards for RNA-seq experiments. *Genome Research* 21: 1543–1551.
- Jimeno S, Luna R, García-Rubio M, Aguilera A. 2006. Tho1, a novel hnRNP, and Sub2 provide alternative pathways for mRNP biogenesis in yeast THO mutants. *Molecular and Cellular Biology* 26: 4387–4398.
- Kammel C, Thomaier M, Sørensen BB, Schubert T, Längst G, Grasser M, Grasser KD. 2013. Arabidopsis DEAD-box RNA helicase UAP56 interacts

- with both RNA and DNA as well as with mRNA export factors. *PLoS ONE* 8: e60644.
- Katahira J. 2012. mRNA export and the TREX complex. *Biochimica et Biophysica Acta* 1819: 507–513.
- Köhler A, Hurt E. 2007. Exporting RNA from the nucleus to the cytoplasm. *Nature Reviews. Molecular Cell Biology* 8: 761–773.
- Kubina J, Geldreich A, Gales JP, Baumberger N, Bouton C, Ryabova LA, Grasser KD, Keller M, Dimitrova M. 2021. Nuclear export of plant pararetrovirus mRNAs involves the TREX complex, two viral proteins and the highly structured 5' leader region. *Nucleic Acids Research* 49: 8900–8922.
- Lamesch P, Berardini TZ, Li D, Swarbreck D, Wilks C, Sasidharan R, Muller R, Dreher K, Alexander DL, Garcia-Hernandez M *et al.* 2012. The Arabidopsis Information Resource (TAIR): improved gene annotation and new tools. *Nucleic Acids Research* 40: D1202–D1210.
- Lanzetta PA, Alvarez LJ, Reinach PS, Candia OA. 1979. An improved assay for nanomole amounts of inorganic phosphate. *Analytical Biochemistry* 100: 95–97.
- Liao Y, Smyth GK, Shi W. 2019. The R package Rsubread is easier, faster, cheaper and better for alignment and quantification of RNA sequencing reads. *Nucleic Acids Research* 47: e47.
- Lolas IB, Himanen K, Grönlund JT, Lynggaard C, Houben A, Melzer M, van Lijsebettens M, Grasser KD. 2010. The transcript elongation factor FACT affects Arabidopsis vegetative and reproductive development and genetically interacts with HUB1/2. *The Plant Journal* 61: 686–697.
- Love ML, Huber W, Anders S. 2014. Moderated estimation of fold change and dispersion for RNA-seq data with DESeq2. *Genome Biology* 15: 550.
- Maniatis T, Reed R. 2002. An extensive network of coupling among gene expression machines. *Nature* 416: 499–506.
- Markusch H, Michl-Holzinger P, Obermeyer S, Thorbecke C, Bruckmann A, Babl S, Längst G, Osakabe A, Berger F, Grasser KD. 2023. ELF1 is a component of the Arabidopsis RNA polymerase II elongation complex and associates with a subset of transcribed genes. *New Phytologist* 238: 113–124.
- Merkle T. 2011. Nucleo-cytoplasmic transport of proteins and RNA in plants. *Plant Cell Reports* 30: 153–176.
- Michl-Holzinger P, Obermeyer S, Markusch H, Pfab A, Ettner A, Bruckmann A, Babl S, Längst G, Schwartz U, Tvardovskiy A *et al.* 2022. Phosphorylation of the FACT histone chaperone subunit SPT16 affects chromatin at RNA polymerase II transcriptional start sites in *Arabidopsis*. *Nucleic Acids Research* 50: 5014–5028.
- Moore MJ, Proudfoot NJ. 2009. Pre-mRNA processing reaches back to transcription and ahead to translation. *Cell* 136: 688–700.
- Mordstein C, Savisaar R, Young RS, Bazile J, Talmane L, Luft J, Liss M, Taylor MS, Hurst LD, Kudla G. 2020. Codon usage and splicing jointly influence mRNA localization. *Cell Systems* 10: 351–362.
- Murashige T, Skoog F. 1962. A revised medium for rapid growth and bioassay with tobacco tissue cultures. *Physiologia Plantarum* 15: 473–497.
- Obermeyer S, Stöckl R, Schnekenburger T, Kapoor H, Stempf T, Schwartz U, Grasser KD. 2023. TFIIS is crucial during early transcript elongation for transcriptional reprogramming in response to heat stress. *Journal of Molecular Biology* 435: 167917.
- Obermeyer S, Stöckl R, Schnekenburger T, Moehle C, Schwartz U, Grasser KD. 2022. Distinct role of subunits of the Arabidopsis RNA polymerase II elongation factor PAF1C in transcriptional reprogramming. *Frontiers in Plant Science* 13: 974625.
- Pacheco-Fiallos B, Vorländer MK, Riabov-Bassat D, Fin L, O'Reilly FJ, Ayala FI, Schellhaas U, Rappsilber J, Plaschka C. 2023. mRNA recognition and packaging by the human transcription-export complex. *Nature* 616: 828–835.
- Pan H, Liu S, Tang D. 2012. HPR1, a component of the THO/TREX complex, plays an important role in disease resistance and senescence in *Arabidopsis*. *The Plant Journal* 69: 831–843.
- Park MY, Wu G, Gonzalez-Sulser A, Vaucheret H, Poethig RS. 2005. Nuclear processing and export of microRNAs in Arabidopsis. *Proceedings of the National Academy of Sciences, USA* 102: 3691–3696.
- Parry G. 2013. Assessing the function of the plant nuclear pore complex and the search for specificity. *Journal of Experimental Botany* 64: 833–845.
- Pfaff C, Ehrnsberger HF, Flores-Tornero M, Sorensen BB, Schubert T, Längst G, Griesenbeck J, Sprunck S, Grasser M, Grasser KD. 2018. ALY RNA-Binding proteins are required for nucleocytoplasmic mRNA transport and modulate plant growth and development. *Plant Physiology* 177: 226–240.
- Piraut JJ, Aguilera A. 1998. A novel yeast gene, THO2, is involved in RNA pol II transcription and provides new evidence for transcriptional elongation-associated recombination. *EMBO Journal* 17: 4859–4872.
- Pühringer T, Hohmann U, Fin L, Pacheco-Fiallos B, Schellhaas U, Brennecke J, Plaschka C. 2020. Structure of the human core transcription-export complex reveals a hub for multivalent interactions. *eLife* 9: e61503.
- Schuller SK, Schuller JM, Prabu JR, Baumgärtner M, Bonneau F, Basquin J, Conti E. 2020. Structural insights into the nucleic acid remodeling mechanisms of the yeast THO-Sub2 complex. *eLife* 9: e61467.
- Shen H. 2009. UAP56 – a key player with surprisingly diverse roles in pre-mRNA splicing and nuclear export. *BMB Reports* 42: 185–188.
- Shi M, Zhang H, Wu X, He Z, Wang L, Yin S, Tian B, Li G, Cheng H. 2017. ALYREF mainly binds to the 5' and the 3' regions of the mRNA *in vivo*. *Nucleic Acids Research* 45: 9640–9653.
- Smith T, Heger A, Sudbery I. 2017. UMI-tools: modeling sequencing errors in Unique Molecular Identifiers to improve quantification accuracy. *Genome Research* 27: 491–499.
- Sørensen BB, Ehrnsberger HF, Esposito S, Pfab A, Bruckmann A, Hauptmann J, Meister G, Merkl R, Schubert T, Längst G *et al.* 2017. The Arabidopsis THO/TREX component TEX1 functionally interacts with MOS11 and modulates mRNA export and alternative splicing events. *Plant Molecular Biology* 93: 283–298.
- Staiger D, Kornel C, Lummer M, Navarro L. 2013. Emerging role for RNA-based regulation in plant immunity. *New Phytologist* 197: 394–404.
- Sträßer K, Hurt E. 2000. Yra1p, a conserved nuclear RNA-binding protein, interacts directly with Mex67p and is required for mRNA export. *EMBO Journal* 19: 410–420.
- Sugiura T, Sakurai K, Nagano Y. 2007. Intracellular characterization of DDX39, a novel growth-associated RNA helicase. *Experimental Cell Research* 313: 782–790.
- Viphakone N, Sudbery I, Griffith L, Heath CG, Sims D, Wilson SA. 2019. Co-transcriptional loading of RNA export factors shapes the human transcriptome. *Molecular Cell* 75: 310–323.e8.
- Wickramasinghe VO, Laskey RA. 2015. Control of mammalian gene expression by selective mRNA export. *Nature Reviews. Molecular Cell Biology* 16: 431–442.
- Wu T, Hu E, Xu S, Chen M, Guo P, Dai Z, Feng T, Zhou L, Tang W, Zhan L *et al.* 2021. CLUSTERPROFILER 4.0: a universal enrichment tool for interpreting omics data. *Innovations* 2: 100141.
- Xie Y, Clarke BP, Kim YJ, Ivey AL, Hill PS, Shi Y, Ren Y. 2021. Cryo-EM structure of the yeast TREX complex and coordination with the SR-like protein Gbp2. *eLife* 10: e65699.
- Xie Y, Gao S, Zhang K, Bhat P, Clarke BP, Batten K, Mei M, Gazzara M, Shay JW, Lynch KW *et al.* 2023. Structural basis for high-order complex of SARNP and DDX39B to facilitate mRNP assembly. *Cell Reports* 42: 112988.
- Xu C, Zhou X, Wen CK. 2015. HYPER RECOMBINATION1 of the THO/TREX complex plays a role in controlling transcription of the REVERSION-TO-ETHYLENE SENSITIVITY1 gene in *Arabidopsis*. *PLoS Genetics* 11: e1004956.
- Xu XM, Meier I. 2008. The nuclear pore comes to the fore. *Trends in Plant Science* 13: 20–27.
- Yamazaki T, Fujiwara N, Yukinaga H, Ebisuya M, Shiki T, Kurihara T, Kioka N, Kambe T, Nagao N, Nishida E *et al.* 2010. The closely related RNA helicases, UAP56 and URH49, preferentially form distinct mRNA export machineries and coordinately regulate mitotic progression. *Molecular Biology of the Cell* 21: 2953–2965.
- Yan Y, Gan J, Tao Y, Okita TW, Tian L. 2022. RNA-binding proteins: the key modulator in stress granule formation and abiotic stress response. *Frontiers in Plant Science* 13: 882596.
- Yelina NE, Smith LM, Jones AME, Patel K, Kelly KA, Baulcombe DC. 2010. Putative Arabidopsis THO/TREX mRNA export complex is involved in transgene and endogenous siRNA biosynthesis. *Proceedings of the National Academy of Sciences, USA* 107: 13948–13953.
- Zenkhusen D, Vinciguerra P, Wyss JC, Stutz F. 2002. Stable mRNP formation and export require cotranscriptional recruitment of the mRNA export factors Yra1p and Sub2p by Hpr1p. *Molecular and Cellular Biology* 22: 8241–8253.

- Zhou Y, Zhou B, Pache L, Chang M, Khodabakhshi AH, Tanaseichuk O, Benner C, Chanda SK. 2019. Metascape provides a biologist-oriented resource for the analysis of systems-level datasets. *Nature Communications* 10: 1523.
- Zuckerman B, Ron M, Mikl M, Segal E, Ulitsky I. 2020. Gene architecture and sequence composition underpin selective dependency of nuclear export of long RNAs on NXF1 and the TREX complex. *Molecular Cell* 79: 251–267.

Supporting Information

Additional Supporting Information may be found online in the Supporting Information section at the end of the article.

- Fig. S1** Amino acid sequence alignment of MOS11 and related sequences of different plant species.
- Fig. S2** Proteins related to MOS11 contain conserved α -helical domains.
- Fig. S3** Recombinant MOS11 proteins and the corresponding circular dichroism spectra.
- Fig. S4** Nuclear localisation of UAP56-mCherry as well as of full-length and truncated MOS11-eGFP fusion proteins.
- Fig. S5** Influence of MOS11 and ALY1 on the ATPase and helicase activity.

Fig. S6 *mos11 aly* triple mutants are clearly affected in rosette and leaf morphology.

Fig. S7 Validation of the cell fractionation and principal component analysis of the RNA-seq analysis.

Fig. S8 Enriched Gene Ontology subterms of the parent term ‘metabolic process’ and their associated transcripts enriched in either nuclei or cytoplasm of *mos11* plants.

Fig. S9 MOS11 binds preferentially to GC-rich RNA.

Fig. S10 Transcripts upregulated upon exposure of Col-0 plants to elevated NaCl concentrations or heat stress are shorter and more GC-rich within their CDS than unaffected transcripts.

Table S1 Oligonucleotides used in this study.

Table S2 Plasmids used in this study.

Table S3 Genes of differentially enriched transcripts.

Please note: Wiley is not responsible for the content or functionality of any Supporting Information supplied by the authors. Any queries (other than missing material) should be directed to the *New Phytologist* Central Office.